photonics

MDPI

Article

A Hybrid Metasurface Filter for Multi-Color Visible Light Communication

Meiyu Qiang [1], Sheng Xie [1,*] and Jia Cong [2,*]

[1] School of Microelectronics, Tianjin University, Tianjin 300072, China
[2] School of Computer and Information Engineering, Tianjin Chengjian University, Tianjin 300392, China
* Correspondence: xie_sheng06@tju.edu.cn (S.X.); congj2015@tju.edu.cn (J.C.)

Abstract

Visible light communication (VLC) has emerged as a highly promising next-generation wireless communication technology, due to its high security, license-free availability and wide-bandwidth resources (400–800 THz). Multi-color visible light communication (MC-VLC), which can carry large amounts of data and increase communication rates, has become a viable route toward high-speed VLC. However, MC-VLC systems are often constrained by inter-channel interference (ICI) caused by the broad spectral overlap of commercial RGB-LEDs (with an overlap ratio of 15–25%), thus severely degrading the signal-to-interference-plus-noise ratio (SINR) and communication reliability. To address this bottleneck, this paper proposes a vertically stacked hybrid metasurface filter formed by an upper square ring–cross Ag structure and a lower I-shaped polysilicon grating, which are separated by a SiO_2 spacer. By exploiting detuned near-field coupling between the localized surface plasmon resonance (LSPR) of the upper cross-shaped metal metasurface and the guided-mode resonance (GMR) of the lower CMOS-compatible polysilicon grating, highly selective narrowband transmissions for red (650 nm), green (550 nm), and blue (450 nm) communication bands are realized. Simulation results indicate that our designed filter achieves transmission rates as high as 90.6%, 94.7% and 91.4% for the three target bands, respectively. It effectively suppresses spectral leakage in non-target bands and significantly reduces ICI, while its compact, subwavelength-scale design also meets the high-density integration requirements of VLC systems. This research provides a novel device solution for realizing low-crosstalk, high-sensitivity and high-speed MC-VLC photodetection systems.

Keywords: MC-VLC; metasurface; filter; LSPR; GMR

1. Introduction

With the rapid advancement of wireless communication technologies, there is a growing demand for high-speed, secure, and anti-interference communication solutions. As an emerging technology, visible light communication (VLC) utilizes the visible spectrum spanning roughly 400 nm to 750 nm as a transmission medium. Leveraging unique advantages—such as the reuse of existing LED lighting infrastructure, no requirement for additional base station construction, superior security compared to Radio Frequency (RF) communication, and license-free wideband resources—VLC has demonstrated great application value in high-speed data transmission and indoor intelligent communication scenarios [1–3]. Among various VLC light sources, red–green–blue Light-Emitting Diodes (RGB-LEDs) have become the core components in supporting high-speed MC-VLC systems, as they can carry data streams in parallel across three independent wavelength channels via wavelength

Check for updates

Received: 28 October 2026
Revised: 23 November 2026
Accepted: 26 November 2026
Published: 27 November 2026

Copyright: © 2026 by the authors. Licensee MDPI, Basel, Switzerland. This article is an open access article distributed under the terms and conditions of the Creative Commons Attribution (CC BY) license.

division multiplexing (WDM) [4]. However, unlike laser diodes, commercial RGB-LEDs exhibit a broad emission spectrum (with a Full Width at Half-Maximum, FWHM, typically exceeding 50 nm) and significant spectral overlap between adjacent color channels (ranging from 15% to 25%). At the receiver side, this overlap results in severe inter-channel interference (ICI), which significantly degrades the signal-to-interference-plus-noise ratio (SINR) and restricts the communication rate and transmission reliability of VLC systems [5,6]. Therefore, MC-VLC receivers must achieve efficient and precise color channel separation to fundamentally overcome this bottleneck.

Currently, MC-VLC systems primarily rely on traditional optical filters (e.g., thin-film dichroic filters and colored glass filters) for color separation, but their performance struggles to meet the demands of high-density integration. Firstly, traditional organic dye or thin-film interference filters suffer from a trade-off between filtering precision and transmission efficiency. They often provide less than 50% crosstalk suppression and involve over 30% energy loss, thus limiting the system's SINR [7]. Secondly, such filters are bulky and difficult to monolithically integrate with photodetectors (PDs), thereby hindering the miniaturization of optical receivers [8]. Furthermore, the stability issues of organic materials under long-term illumination or in high-temperature environments restrict their application scenarios [9].

In recent years, metasurfaces—artificial two-dimensional materials composed of sub-wavelength units—have provided a novel technical path for constructing lightweight and integrated spectral filtering devices, due to their ability to flexibly manipulate key parameters such as amplitude, phase, and polarization [10,11]. However, the existing metasurface technologies still face numerous challenges when directly applied to MC-VLC channel separation. For instance, although metasurfaces based on single-layer silicon structures have achieved multi-channel radiation control, their transmittance in the visible band is often low due to material absorption and scattering loss, and their filtering precision is insufficient to effectively resolve crosstalk [12]. Other studies, such as that on the multi-color full-polarization control metasurface proposed by the group of Li [13], achieved wavelength demultiplexing but operated primarily in the mid-infrared region (2–10 μm), failing to match the visible bands of RGB-LEDs. Additionally, current research on dual-layer metasurfaces focuses largely on broadband absorption [14], lacking specialized designs for narrowband and high-transmission filtering requirements. In summary, the existing technologies generally suffer from common issues such as poor filtering precision, low transmittance and difficulties in integration with standard CMOS processes.

Up to now, considerable efforts have been devoted to developing metasurface-based RGB spectral filters operating in the visible band, and they can be roughly divided into all-dielectric, plasmonic, and hybrid metal–dielectric categories. All-dielectric metasurface filters based on Mie resonances can achieve low ohmic loss, yet they usually demand high-aspect-ratio nanostructures and suffer from relatively low transmittance for multi-channel RGB filtering [15]. Pure plasmonic RGB filters benefit from a simple unit-cell geometry and flexible spectral tuning, but intrinsic metallic ohmic loss severely limits their peak transmittance, and crosstalk suppression remains challenging [16]. Hybrid metal–dielectric metasurfaces combine the merits of plasmonic light confinement and dielectric low-loss resonance, offering a promising route toward high-efficiency RGB filtering. Nevertheless, most of the reported hybrid RGB designs are optimized for structural color imaging rather than MC-VLC receivers, thus lacking deliberate detuned-mode designs for low-crosstalk wavelength-division multiplexing communication scenarios [17]. Beyond absorptive color filters, metasurface-based color routers have recently emerged for efficient RGB color separation on CMOS image sensors [18,19], and BIC metasurfaces have been widely exploited for high-Q spectral control [20].

To overcome these issues, this paper proposes a hybrid metasurface filter structure that vertically integrates a top-layer metallic nanoantenna array with a bottom-layer polysilicon waveguide grating. Our core design philosophies are spectral detuning and mode hybridization by engineering the interaction between the top-layer broadband LSPR and the bottom-layer narrowband GMR. A Fano-like interference effect is utilized to induce an ultra-narrow high-transmission window within a broadband reflective background for RGB visible light communication compared with previously reported metasurface spectrometric filters in Refs. [21–23], which provides an alternative strategy for narrowband spectral filtering. Simulation results demonstrate that this structure achieves over 90% transmission efficiency across the red, green and blue spectral bands while significantly suppressing inter-channel interference. More importantly, the design employs CMOS-compatible polysilicon materials, providing a practical solution for the monolithic integration of filters with silicon-based photodetectors, which is expected to significantly enhance the overall performance and integration level of MC-VLC receivers.

2. Design Concept and Working Principle

2.1. Architectural Overview and Innovation Concept

To address the aforementioned requirements, we propose a novel hybrid plasmonic–photonic metasurface architecture that vertically integrates a metallic nanoantenna array with a polysilicon grating. As illustrated in Figure 1, the device is constructed on a silicon (*Si*) substrate. In addition to providing mechanical support, the Si substrate can serve directly as the active region of the photodetector in monolithic integration schemes. An intermediate SiO_2 layer with a thickness of 350 nm is employed to separate the substrate from the main body of the filter.

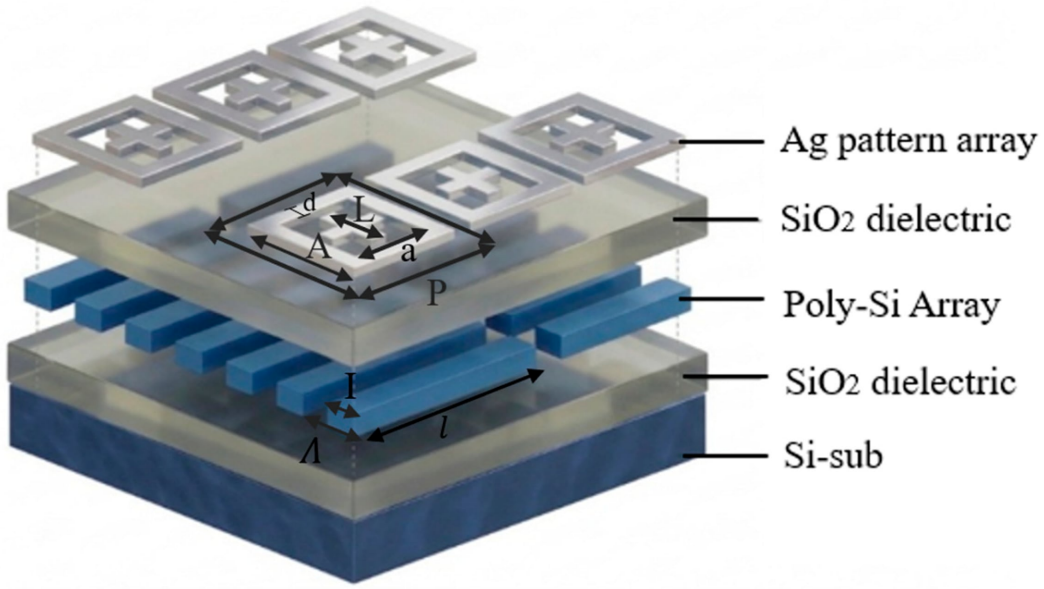


Figure 1. A schematic diagram of the dual-layer metasurface structure.

The functional layer of the filter adopts a vertically stacked metal–dielectric–semiconductor (MDS) structure, utilizing a hybrid metasurface to achieve cascaded modulation of the incident light. The top layer of the metasurface structure is formed of sub-wavelength metallic patterns. By optimizing geometric parameters such as the dimension, duty cycle and period, the localized surface plasmon resonance (LSPR) effect is excited within the target red–green–blue (RGB) bands. At this stage, the energy of incident white light becomes highly localized at the metal–insulator interface, particularly in the "hotspot" regions at the

edges of the patterns. This layer serves as a preliminary spectral selector for the target bands while effectively suppressing background stray light through strong field confinement.

The bottom layer of the metasurface structure is composed of periodic units made of polysilicon, which functions as a high-selectivity wavelength filter by exciting guided mode resonance (GMR). Its ultra-narrow resonance bandwidth allows for secondary refinement of the transmission spectrum, further eliminating the noise outside the target bands. The intermediate dielectric layer between the top and the bottom layers acts as a mode matcher and an energy channel, mediating the near-field evanescent wave coupling between these two layers.

Physically, the direct scattering channel (the bright mode) and the resonance-aided channel (the dark mode) undergo strong coupling via the intermediate layer. When the phase-matching condition is satisfied, their destructive interference induces an extremely narrow transparency window within the broadband reflective background. Consequently, this hybrid structure achieves high transmittance that significantly exceeds those of single-layer plasmonic structures.

By precisely adjusting the thickness of the intermediate dielectric layer, efficient evanescent coupling from the LSPR mode to the GMR mode can be achieved. When optimal mode matching between these two excitation patterns is reached, the formation of this hybrid resonance window greatly boosts the optical response within the target bands, enabling narrowband filtering with high transmittance and high spectral purity for the RGB communication channels.

2.2. Theoretical Analysis: Temporal Coupled-Mode Theory (TCMT)

To provide a rigorous quantitative analysis of the hybridization mechanism, we introduce temporal coupled-mode theory (TCMT) [24,25]. The dual-layer system can be modeled as two coupled resonators interacting with input and output ports. Here, we use a_1 and a_2 to represent the complex amplitudes of the LSPR mode (Mode 1) and the GMR mode (Mode 2), respectively. The system evolution is described by the following coupled differential equations:

$$\frac{d}{dt}\begin{pmatrix} a_1 \\ a_2 \end{pmatrix} = \begin{pmatrix} -i\omega_1 - \gamma_1 & i\kappa \\ i\kappa & -i\omega_2 - \gamma_2 \end{pmatrix}\begin{pmatrix} a_1 \\ a_2 \end{pmatrix} + \begin{pmatrix} \sqrt{\gamma_{r1}} \\ 0 \end{pmatrix} S_{in}. \quad (1)$$

Here ω_1 and ω_2 are the resonant angular frequencies of the LSPR and the GMR modes, respectively ($\omega_1 \neq \omega_2$ due to the detuning condition). γ_1 and γ_2 represent the total decay rates, comprising the radiative decay (γ_{rad}) and the non-radiative/ohmic losses (γ_{nrad}). κ is the near-field coupling coefficient, whose magnitude varies exponentially with the spacer thickness t. S_{in} denotes the amplitude of the incident wave. γ_{r1} is the radiative decay rate of the bright LSPR mode (Mode 1). It describes the energy leakage rate from the LSPR resonator to the input free-space port. Since Mode 2 (GMR dark mode) cannot be directly excited by incident light, there is no corresponding γ_{r2} term in the coupling-mode equations [25].

We assume that the direct excitation of the dark mode a_2 is negligible relative to that of the bright mode a_1. The transmission coefficient t can be derived from the output field s_{out}. By solving the system of equations in the frequency domain, the analytical expression for the transmission spectrum is obtained as follows:

$$T(\omega) = \left| \frac{S_{out}}{S_{in}} \right|^2 = \left| 1 - \frac{\gamma_{r1}}{i(\omega - \omega_1) + \gamma_1 + \frac{\kappa^2}{i(\omega-\omega_2)+\gamma_2}} \right|^2 \quad (2)$$

This analytical expression (Equation (2)) uncovers the physical origin of the observed spectral response, arising from the coupling and mutual modulation between narrowband

GMR resonance and broadband LSPR response. The step-by-step derivation of Equation (2) from Equation (1) and the parameter extraction procedure are provided in Note S3 of the Supplementary Materials.

When $\omega \approx \omega_2$, the denominator of the coupling term, defined as $\boldsymbol{\kappa}^2/[\boldsymbol{i}(\boldsymbol{\omega} - \boldsymbol{\omega}_2) + \boldsymbol{\gamma}_2]$ in Equation (2), is minimized, thereby maximizing the total impedance term $\boldsymbol{i}(\boldsymbol{\omega} - \boldsymbol{\omega}_1) + \boldsymbol{\gamma}_1 + \frac{\boldsymbol{\kappa}^2}{\boldsymbol{i}(\boldsymbol{\omega}-\boldsymbol{\omega}_2)+\boldsymbol{\gamma}_2}$. Physically, the coupling term accounts for the energy transfer pathway mediated by near-field mode hybridization between LSPR and GMR resonators. The total impedance term characterizes the overall spectral response of the hybrid coupled resonator system, combining the intrinsic loss of Mode 1 and the mode–mode coupling contribution. A large magnitude of this total impedance term suppresses direct reflection and produces a reflection dip (i.e., a transmission peak) within the reflection valley. By finely tuning k (via the spacer thickness t) and the detuning $\Delta\omega$, the lineshape is tailored to form a symmetric, high-efficiency transparency window. This effectively suppresses the intrinsic losses of the plasmonic layer and sharpens the spectral response of the composite system. This theoretical model is in excellent agreement with our FDTD simulation results, confirming that the high performance of the proposed filter indeed originates from the precise interference control between the plasmonic and photonic modes.

2.3. Functional Unit Design and Physical Mechanism

Three filters with identical architecture but independently optimized geometric parameters were designed for the red, green, and blue channels. The geometric parameters of each functional layer were rigorously optimized based on full-wave simulations to independently target the red (650 nm), green (550 nm), and blue (450 nm) communication channels. The specific design parameters for these three channels are presented in Table 1.

Table 1. Parameter data table for LSPR and GMR layers.

nm	P	A	a	L	d	l	I	Λ
Red	675	585	560	500	25	610	190	350
Green	575	505	480	420	20	490	130	300
Blue	475	430	410	350	20	390	90	290

Taking the red channel filter as an example, the design basis is elaborated as follows:

For the design of 650 nm red light selection, the transmission peaks of the top and the bottom metasurface structures are engineered to be separated by 40 nm. Specifically, the peak wavelength of the top metasurface is designed at 630 nm, while the peak of the bottom metasurface corresponds to 670 nm. By relying on the spectral overlap of these two optical responses for wavelength selection, a significantly narrower bandwidth can be achieved. Furthermore, the coupling efficiency between these two layers is regulated by optimizing the thickness of the intermediate dielectric layer, which in turn enhances the overall transmittance of the filter. The filter structure is vertically integrated from top to bottom, with the key parameters and functions of each layer described below:

The top layer is patterned for a 20 nm thick silver (Ag) thin film, which utilizes a composite square ring–cross unit cell. Compared to gold or aluminum, silver exhibits lower ohmic losses within the visible spectrum. The square ring–cross geometry was selected due to its large scattering cross-section and flexible tunability. The resonance condition of the LSPR mode is primarily determined by the effective dipole length. According to dipole approximation theory, the resonant wavelength λ_{LSPR} is linearly related to the structural dimensions and the refractive index of the surrounding environment:

$$\lambda_{LSPR} \approx n_{eff}(L + \delta). \quad (3)$$

where n_{eff} is the effective refractive index of the interface, L is the arm length of the cross, and δ is the phase correction factor. Considering that the Ag nanostructures are embedded at the interface between the SiO_2 capping layer and the air, the effective refractive index n_{eff} is co-modulated by the media on both sides. Furthermore, the outer square ring structure (parameter A) not only broadens the spectral capture range but also introduces a phase correction term δ through electromagnetic interaction with the cross structure.

For the top metasurface targeting a wavelength of 630 nm, we set the unit cell period to $P = 675$ nm, the outer side length of the square ring to $A = 585$ nm, the inner side length to $a = 560$ nm, the optimized cross arm length to 500 nm, and the linewidth d to 25 nm. Figure 2 illustrates the transmission efficiency of the RGB communication channels in the presence of a single LSPR layer, based on the parameter design in Table 1.

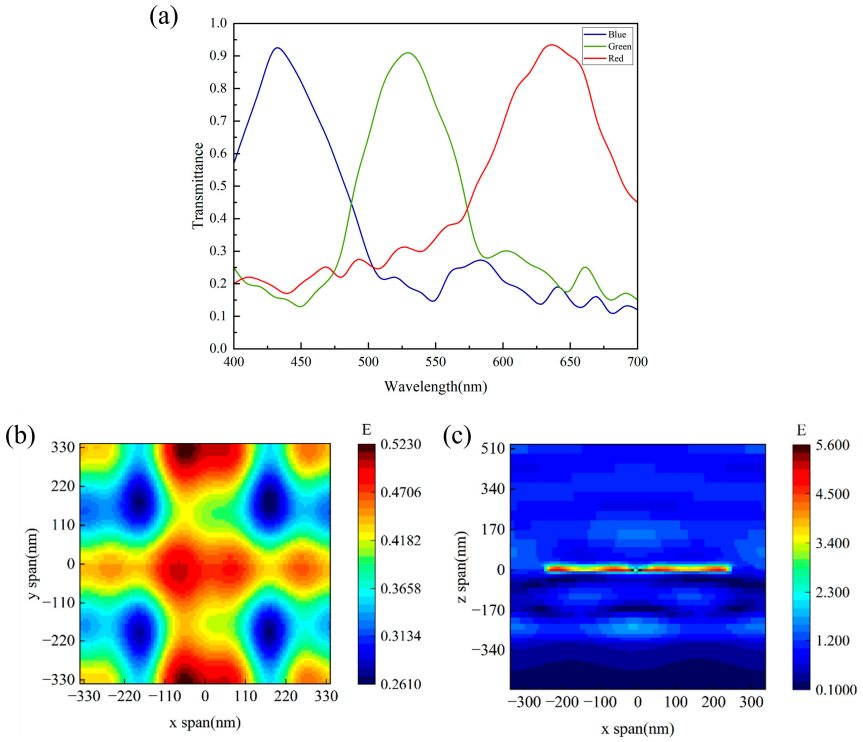


Figure 2. Transmittance of the top layer for RGB communication channels under the parameter design in Table 1. (**a**) Transmission spectra; (**b**) the xy-cross-section electric field intensity distribution and (**c**) xz-cross-section electric field intensity distribution, calculated at the red resonant wavelength of 630 nm under normal incidence from the air side.

The narrowband high-transmission characteristic of this periodic Ag square ring–cross metasurface at 630 nm is attributed to the excitation of the "transmission-enhanced" localized surface plasmon resonance (LSPR) mode at this specific wavelength. The excited magnetic dipole (MD) and electric dipole (ED) resonances undergo coherent superposition through the precise design of the composite unit cell geometry, which satisfies the generalized Kerker effect and thereby significantly suppresses backscattering. Simultaneously, the near-field coupling of gap plasmons between the cross arms and the square ring further enhances the capture and re-radiation efficiency of the optical field, ultimately achieving an anomalous transmission enhancement exceeding 90% at the resonant wavelength.

The bottom-layer metasurface employs heavily doped p-type polysilicon (poly-Si) with a thickness of 110 nm. For the 670 nm wavelength selection, an I-shaped (rectangular) periodic sub-wavelength array is utilized, where the side lengths of the structure l and I are 390 nm and 190 nm, while the period P is 350 nm. Polysilicon was selected due to its

high refractive index ($n \approx 3.48$), and it serves as a standard material in CMOS processes, offering fabrication compatibility superior to that of amorphous silicon or other specialized dielectrics. This layer operates as a leaky-mode waveguide, and when the phase-matching condition is satisfied, incident light is diffracted into the waveguide layer and couples into a guided mode, which subsequently leaks back into the free-space continuum. The phase-matching condition for the GMR effect is governed by the following grating equation:

$$\beta = k_0 \sin\theta + m\frac{2\pi}{\Lambda} = k_0 n_{eff}. \quad (4)$$

Here, $k_0 n_{eff}$ is the propagation constant of the guided mode, k_0 is the free-space wavenumber, n_{eff} is the effective refractive index of the slab waveguide mode, θ is the angle of incidence, m is the diffraction order (typically $m = \pm 1$), and Λ (or P) is the grating period. To support the TE-polarized GMR mode at 670 nm (slightly detuned from the LSPR peak), the grating period was optimized to 350 nm with a meticulously adjusted duty cycle. This resonance acts as the "dark" discrete state within the coupled system. Figure 3 illustrates the transmission spectra for the standalone bottom I-shaped grating for the RGB communication channels under the design parameters summarized in Table 1.

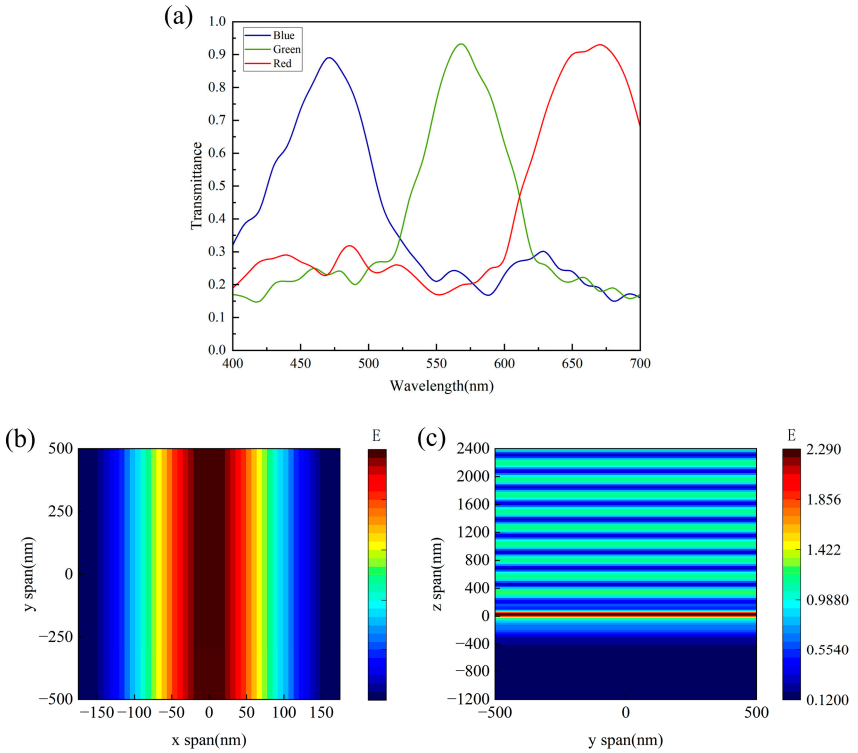


Figure 3. Transmittance of the bottom layer for the RGB communication channels under the parameter design in Table 1. (**a**) Transmission spectra; (**b**) the xy-cross-section electric field intensity distribution and (**c**) xz-cross-section electric field intensity distribution, calculated at the red resonant wavelength of 670 nm under normal incidence from the air side.

An intermediate silicon dioxide SiO_2 layer is employed to separate the top and bottom metasurface structures, providing a critical tuning parameter for both phase and coupling control. The spacer thickness t serves as the system's primary tuning knob. It governs not only the overlap integral between the evanescent field tail of the top LSPR and the bottom GMR field but also the accumulated phase delay ϕ as waves propagate between these two layers.

3. Simulation Results and Analysis: Validation of Design and Operating Principles

To verify the rationality of the core structural design and the feasibility of the synergistic operating mechanism, full-wave numerical simulations of the proposed dual-layer metasurface filter's spectral response were performed using the Finite-Difference Time-Domain (FDTD) method([Lumerical FDTD], version [2023 R1.1], [Ansys Inc.], [Vancouver, BC], [Canada]); the specific simulation setup is shown in Table 2. By conducting a quantitative analysis of the transmission spectra, bandwidth characteristics, and coupling efficiencies for the red, green and blue target channels, the effectiveness of spectral detuning and the near-field hybridization mechanism were fully validated from a performance perspective.

Table 2. FDTD simulation settings and material parameters.

Item	Specification
Method	FDTD method
Boundary conditions	x(y) periodic boundary conditions; z PML
Light Source	400–700 nm; θ = 0°; TE polarization
Mesh	Metal/nanostructure: 2–5 nm; SiO_2 and Si substrate: 10 nm
Materials	Ag: CRC optical constants (curve-fitted as Figure S1); poly-Si, SiO_2, Si: Palik
Monitor	Power monitor at the SiO_2/Si interface
Transmittance	Power coupled into the Si active region
Energy conservation check	Reflection and absorption spectra added (Figures S2–S4)

3.1. Coupling Conditions and Sensitivity Analysis of Spacer-Layer Modulation

To verify the fundamental role of the intermediate spacer layer as a phase matcher and an energy channel, we analyzed the spectral response under varying spacer thicknesses. Figure 4 illustrates how the SiO_2 spacer-layer thickness modulates the coupling efficiency between the top and bottom metasurfaces for red, green and blue channels. At optimal specific thickness, the round-trip phase condition facilitates constructive interference for forward-propagating waves while simultaneously suppressing reflection via destructive interference, thereby maximizing the transmittance of the induced transparency window.

As shown in Figure 4a–c, the simulation results demonstrate that the coupling efficiency exhibits a high degree of dependence on the spacer thickness, validating the physical nature of near-field coupling. If the SiO_2 layer is too thin, the ohmic losses from the metallic layer are dominant, resulting in resonance peak broadening and a reduction in transmittance. Conversely, if the SiO_2 layer is too thick, the evanescent field overlap between the top and bottom layers weakens, hindering the formation of a robust hybrid mode and causing the spectrum to split into two independent weak peaks. Only at the optimized design thicknesses (120 nm for red, 180 nm for green, and 150 nm for blue) do the excited modes satisfy the phase-matching condition to induce a near-perfect transmission window. This observed trend aligns closely with the predictions from TCMT described in Section 2.2, further substantiating the theoretical integrity of the device design.

It can be seen that small periodic ripples appear in the non-target wavelength range for all calculated transmission spectra. These oscillations arise from Fabry–Pérot multi-beam interference within the stacked metal–dielectric layers. Since the transmittance in this spectral range is relatively low, tiny absolute variations lead to visible relative fluctuations.

This phenomenon is an intrinsic optical characteristic of the multilayer architecture and has been widely observed in related metasurface filter studies [26].

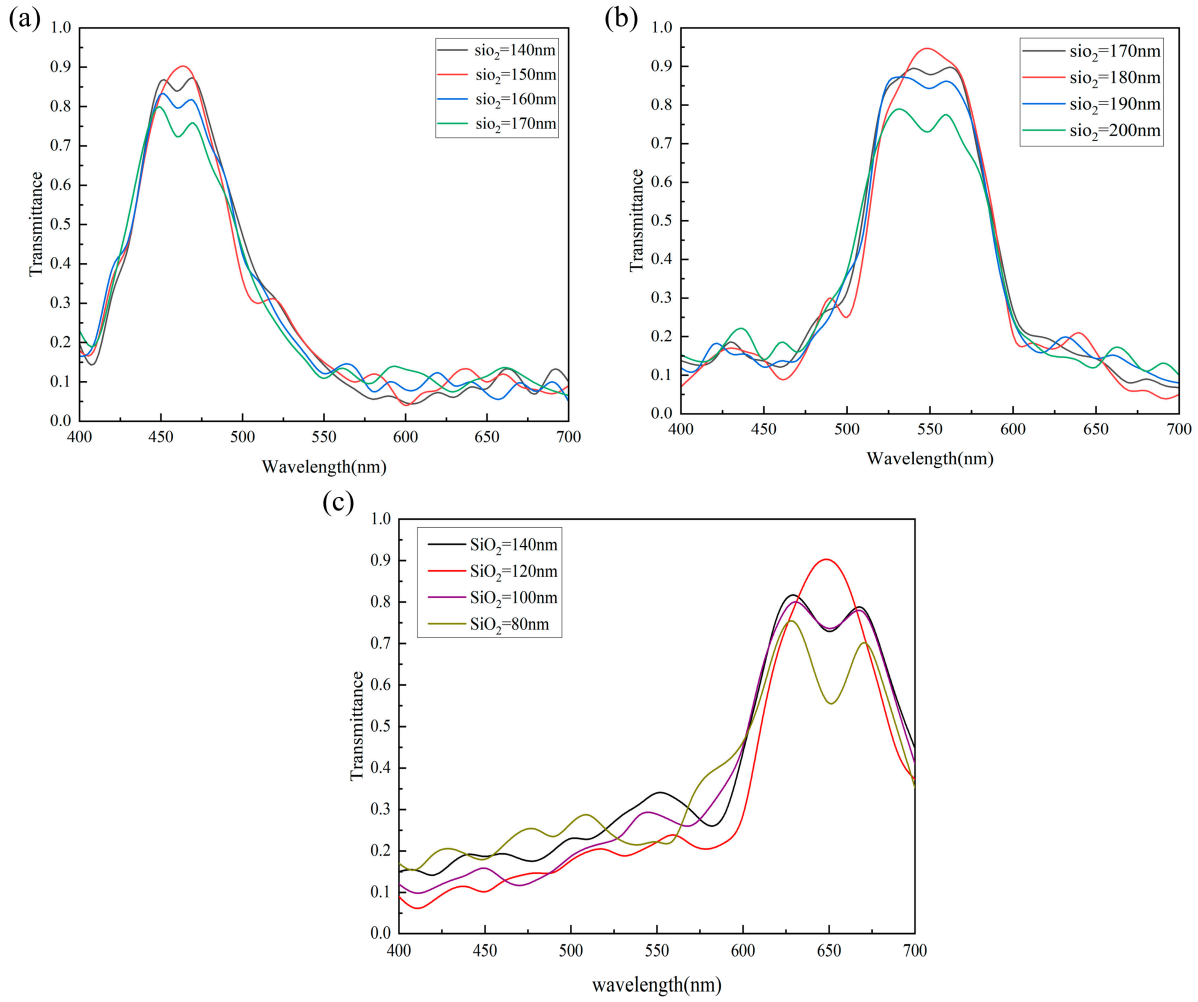


Figure 4. Influence of various SiO_2 layer thicknesses on the overall transmission performance of the dual-layer metasurface structure: (**a**) influence on blue light transmittance; (**b**) influence on green light transmittance;(**c**) influence on green light transmittance

3.2. Transmission Spectra of RGB Communication Channels and Verification of Efficiency Enhancement

Furthermore, a full-spectrum scan was performed on the filters designed for the red (650 nm), green (550 nm) and blue (450 nm) communication bands. The simulation results shown in Figure 5 clearly demonstrate the significant advantage of the dual-layer structure in enhancing transmission efficiency.

With an optimal intermediate SiO_2 spacer thickness of 120 nm, high-efficiency coupling occurs between the top-layer Ag metasurface (peaking at ~630 nm) and the bottom-layer poly-Si grating (peaking at ~670 nm). The results indicate that the filter achieves a peak transmittance of 91.4% at 650 nm. The green channel exhibits optimal performance with a spacer thickness of 180 nm, reaching a peak transmittance of up to 94.7%. This demonstrates that the high-refractive-index advantage of polysilicon is fully leveraged in the green spectral band, resulting in highly precise mode matching. Despite the intrinsic interband absorption of silicon at shorter wavelengths, the dual-layer structure effectively redistributes the optical field, localizing energy primarily within the dielectric region to minimize loss pathways

within the silicon. Consequently, this channel maintains a high transmittance of 90.6% at a spacer thickness of 150 nm.

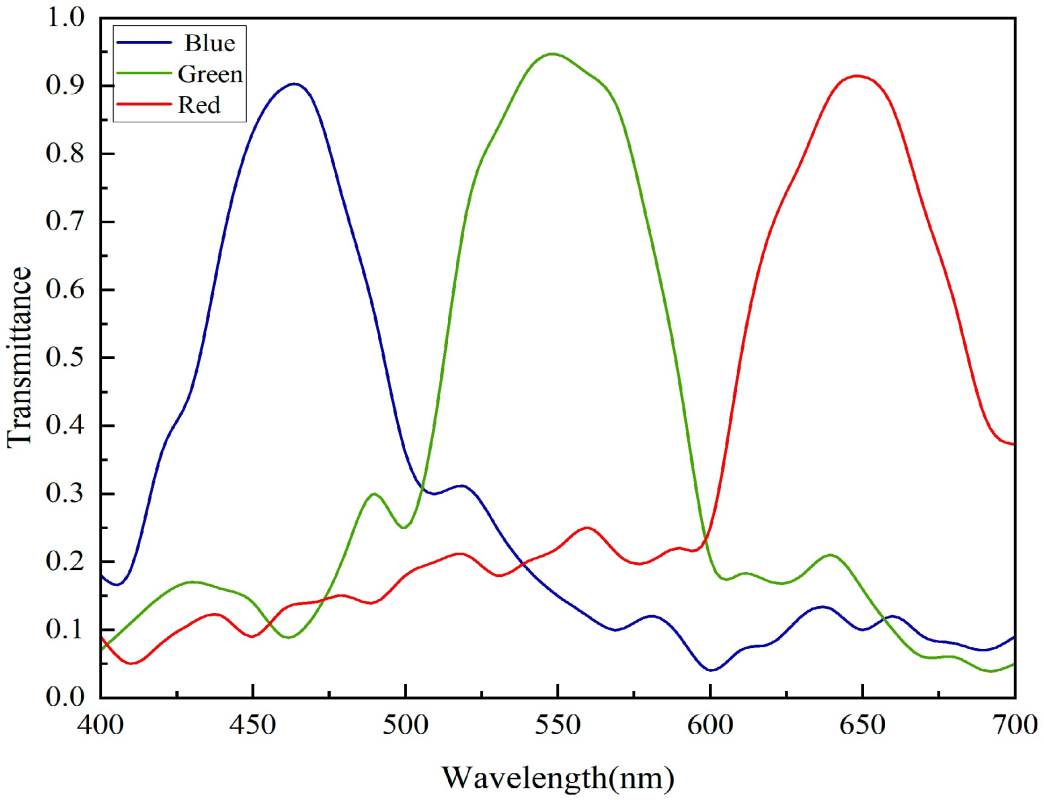


Figure 5. Overall filtering performance of the dual-layer metasurface structure (400–700 nm).

Compared with the single-layer silicon nanopillar filters reported in Ref. [27], our dual-layer hybrid structure achieves transmittance enhancement in different target bands. A substantial transmittance enhancement is observed in the blue band, while moderate performance gains are obtained for the red and green bands. These results demonstrate that the LSPR-GMR hybrid mode can alleviate Mie-resonance scattering losses in single-layer dielectric structures and ohmic losses in pure plasmonic structures, which is beneficial for high-efficiency photon energy transfer and tunneling.

3.3. Narrowband Filtering Characteristics and Validation of the "Detuned Design" Principle

Spectral selectivity (i.e., bandwidth) is a critical metric for evaluating the device's capability to suppress ICI in MC-VLC. The simulation results fully validate the effectiveness of the detuned design in compressing the bandwidth.

From a system perspective, by suppressing inter-channel spectral leakage while maintaining a peak transmittance above 90%, the proposed filter is expected to markedly improve the received SINR and, correspondingly, the BER of an MC-VLC link; a complete system-level evaluation is left for future work.

From the perspective of detuned mode design, there exists an inherent trade-off among spectral bandwidth, peak transmittance, and crosstalk suppression, governed by the wavelength detuning $\Delta\lambda$ between the LSPR and GMR resonances. For the three RGB working channels, the detuning parameters are individually optimized according to the material loss characteristics at different wavelengths, following the design priority of "crosstalk suppression first, while ensuring high transmittance" for MC-VLC receivers.

Simulation data indicates that single-layer metasurface structures exhibit relatively broad resonance peaks, with a FWHM typically exceeding 100 nm [15,16], which fails to meet the requirements for high-density wavelength division multiplexing (WDM). In contrast, by introducing mode interference in the dual-layer architecture, the FWHMs of the transmission windows for the three RGB channels are compressed.

As observed from the spectral profiles, the transmittance decays rapidly to negligible levels outside the target bands. This steep roll-off characteristic confirms that the hybrid mode not only enhances the transmission of target wavelengths but also effectively suppresses background stray light through destructive interference. For instance, the transmittance of the green and blue bands is suppressed to extremely low levels in the red light filter, thereby ensuring exceptional color purity. Table 3 compares the performance of this filter with that of other reported filters, and the results show that our proposed filter exhibits excellent performance.

Table 3. Performance comparison of various filter types.

Reference	Filter Type	Central Wavelength (B/G/R, nm)	Peak Transmittance (B/G/R)	FWHM (nm)	Main Features
This work	Hybrid metal–dielectric metasurface	450/550/650	90.6/94.7/91.4	70/70/75	Dual-layer LSPR-GMR detuned coupling; CMOS-compatible; designed for MC-VLC receiver
Ref. [15]	All-dielectric a-Si metasurface	450/550/650	60/50/90	All >100	Mie-resonance-based RGB filtering; high-aspect-ratio nanostructures for CMOS image sensors
Ref. [28]	All-dielectric TiO_2 metasurface	410/500/600	68/72/70	70/80/110	Birefringent TiO_2 nanopillar metasurface; switchable additive/subtractive filtering; low ohmic loss
Ref. [16]	Plasmonic Al X-shaped nanoantenna	474/525/684	40/41/66	All >100	Al X-shaped plasmonic nanoantenna; transmission-mode color filter; limited peak transmittance caused by ohmic loss
Ref. [29]	Plasmonic Al nanohole array	450/550/650	70/70/85	80/60/>100	Silver plasmonic nano-array with dual orthogonal LSPR modes; still limited by intrinsic silver ohmic loss
Ref. [17]	Hybrid Al-TiO_2 metasurface	452/530/635	84/80/73	42/67/67	Al-TiO_2 hybrid metasurface; CMOS-compatible; optimized for structural-color imaging instead of VLC communication
Ref. [30]	Hybrid Ag-Tio_2 metasurface	450/532/635	80/65/72	Not reported	Al-TiO_2 hybrid plasmonic–dielectric metasurface; low spectral crosstalk; designed for structural-color print and holography instead of MC-VLC communication

4. Discussion

In the present work, the performance of a dual-layer hybrid metasurface filter composed of an Ag plasmonic nanoantenna array, a SiO_2 spacer, and a poly-Si grating on a Si substrate was simulated and analyzed. By integrating the localized plasmonic effects of the Ag metasurface with the guided-mode resonance (GMR) effects of the poly-Si grating through the intermediate SiO_2 spacer, the proposed structure achieves narrowband high-efficiency transmission: peak transmittances of 91.4%, 94.7%, and 90.6% at 650, 550, and 450 nm, with FWHMs of only 70–75 nm. This simultaneous achievement of high transmittance and narrow bandwidth indicates that the dual-layer architecture breaks the intrinsic trade-off of single-layer resonators, where the same mode governs both wavelength selection and energy dissipation: in our design, the GMR layer is responsible for spectral selectivity while the LSPR layer primarily provides field localization, such that the Mie-scattering loss of dielectric structures and the ohmic loss of metallic structures are alleviated simultaneously. Compared with all-dielectric metasurface filters (peak transmittances of 50–72% and FWHMs exceeding 100 nm [15,28]) and pure plasmonic filters (40–85% [16,29]), the proposed filter offers substantially higher in-band throughput and sharper spectral roll-off, and, unlike previously reported hybrid filters designed for color imaging (Refs. [17,30]), its optimization target is inter-channel crosstalk suppression in MC-VLC receivers rather than color gamut. It should be noted that the blue channel exhibits the smallest performance margin, owing to the interband absorption of silicon at short wavelengths, so further improvements are expected mainly from reducing the metal loss rather than re-optimizing the coupling geometry. In addition, parameter sweeping simulations of the spacer thickness were conducted to optimize the structural design; the steep thickness dependence confirms the near-field coupling mechanism but also implies that a fabrication tolerance of a few nanometers must be guaranteed, and the present analysis assumes normal incidence and TE polarization, which should be extended to angular- and polarization-insensitive designs for practical unpolarized LED links. The proposed device exhibits potential value for application in CMOS-integrated photodetectors of multi-color visible light communication systems. While the current study focused on device-level passive filtering, future developments could extend the evaluation to the system level, where the SINR and bit-error-rate (BER) performance of multi-channel VLC links have been widely investigated [3,4]. Therefore, incorporating the proposed filter into a realistic RGB-LED VLC link could enable quantitative system-level verification and further expand its practical applicability.

5. Conclusions

In summary, a dual-layer hybrid metasurface filter integrating LSPR and GMR effects is proposed for MC-VLC channel separation. The simulation results demonstrate peak transmittances of 91.4/94.7/90.6% with FWHMs of 70–75 nm for the RGB channels, verifying the effectiveness of the detuned design. Upon integration with CMOS photodetectors, the filter is expected to improve the SNR of the photocurrent and suppress inter-channel crosstalk, providing a practical design path for compact MC-VLC receivers. Future work will extend the device-level study to a complete system-level evaluation, quantifying the SINR and BER performance of a realistic RGB-LED VLC link.

Supplementary Materials: The following supporting information can be downloaded at: https://www.mdpi.com/article/10.3390/photonics13121127/s1.

Author Contributions: Conceptualization, M.Q. and J.C.; methodology, M.Q., J.C. and S.X.; software, M.Q.; validation, M.Q.; formal analysis, M.Q. and J.C.; investigation, M.Q. and J.C.; resources, S.X.; data curation, M.Q.; writing—original draft preparation, M.Q. and S.X.; writing—review and editing,

S.X.; visualization, M.Q.; supervision, S.X.; project administration, J.C.; funding acquisition, S.X. All authors have read and agreed to the published version of the manuscript.

Funding: This research received no external funding.

Data Availability Statement: The raw data supporting the conclusions of this article will be made available by the authors on request.

Conflicts of Interest: The authors declare no conflict of interest.

References

1. Ge, P.; Ling, X.; Wang, J.; Liang, X.; Li, S.; Zhao, C. Optical Filter Bank Modeling and Design for Multi-Color Visible Light Communications. *IEEE Photonics J.* **2021**, *13*, 1–19. [CrossRef]
2. Pergoloni, S.; Biagi, M.; Cusani, R.; Scarano, G. Space-time multichannel adaptive filtering scheme for VLC color cross-talk equalization. *Opt. Express* **2018**, *26*, 19750–19761. [CrossRef] [PubMed]
3. Cui, L.; Tang, Y.; Jia, H.; Luo, J.; Gnade, B. Analysis of the Multichannel WDM-VLC Communication System. *J. Light. Technol.* **2016**, *34*, 5627–5634. [CrossRef]
4. Kottke, C.; Habel, K.; Langer, K.D. 803 Mbit/s visible light WDM link based on DMT modulation of a single RGB LED luminary. In Proceedings of the OSA/OFC/NFOEC, Los Angeles, CA, USA, 6–10 March 2011; pp. 1–3.
5. Rajbhandari, S.; Haas, H.; Xie, E.; McKendry, J.J.D.; Herrnsdorf, J.; Gu, E.; Dawson, M.D.; O'BRien, D.; Chun, H.; Faulkner, G.; et al. High-Speed Integrated Visible Light Communication System: Device Constraints and Design Considerations. *IEEE J. Sel. Areas Commun.* **2015**, *33*, 1750–1757. [CrossRef]
6. Tsonev, D.; Videv, S.; Haas, H. Light fidelity (Li-Fi): Towards all-optical networking. In Proceedings of the SPIE Opto, San Francisco, CA, USA, 4–6 February 2014.
7. Piegari, A.; Flory, F. *Optical Thin Films and Coatings from Materials to Applications*; Woodhead Publishing Limited: Cambridge, UK, 2013.
8. Macleod, H.A. *Thin-Film Optical Filters*, 5th ed.; CRC Press: Boca Raton, FL, USA, 2017.
9. Burgos, S.P.; Yokogawa, S.; Atwater, H.A. Color imaging via nearest neighbor hole coupling in plasmonic color filters integrated onto a complementary metal-oxide semiconductor image sensor. *ACS Nano* **2013**, *7*, 10038–10047. [CrossRef] [PubMed]
10. Arbabi, A.; Horie, Y.; Ball, A.J.; Bagheri, M.; Faraon, A. Subwavelength-thick lenses with high numerical apertures and large efficiency based on high-contrast transmitarrays. *Nat. Commun.* **2015**, *6*, 7069. [CrossRef] [PubMed]
11. Pfeiffer, C.; Grbic, A. Metamaterial Huygens' surfaces. In Proceedings of the 2013 IEEE MTT-S International Microwave Symposium Digest (MTT), Seattle, WA, USA, 2–7 June 2013; pp. 1–4.
12. Yang, W.; Xiao, S.; Song, Q.; Liu, Y.; Wu, Y.; Wang, S.; Yu, J.; Han, J.; Tsai, D.-P. All-dielectric metasurface for high-performance structural color. *Nat. Commun.* **2020**, *11*, 1864. [CrossRef] [PubMed]
13. Chen, J.; Yu, F.; Liu, X.; Bao, Y.; Chen, R.; Zhao, Z.; Wang, J.; Wang, X.; Liu, W.; Shi, Y.; et al. Polychromatic full-polarization control in mid-infrared light. *Light Sci. Appl.* **2023**, *12*, 105. [CrossRef] [PubMed]
14. Zhou, Y.; Qin, Z.; Liang, Z.; Meng, D.; Xu, H.; Smith, D.R.; Liu, Y. Ultra-broadband metamaterial absorbers from long to very long infrared regime. *Light Sci. Appl.* **2021**, *10*, 138. [CrossRef] [PubMed]
15. Berzinš, J.; Fasold, S.; Pertsch, T.; Bäumer, S.M.B.; Setzpfandt, F. Submicrometer Nanostructure-Based RGB Filters for CMOS Image Sensors. *ACS Photonics* **2019**, *6*, 1018–1025. [CrossRef]
16. Shafiq, R.; Daud Khan, A.; Al-Harbi, F.F.; Ali, F.; Armghan, A.; Asif, M.; Ur Rehman, A.; Mousa Ali, E.; Arpanaei, F.; Alibakhshikenari, M.; et al. Optical Transmission Plasmonic Color Filter with Wider Color Gamut Based on X-Shaped Nanostructure. *Photonics* **2022**, *9*, 209. [CrossRef]
17. Soliman, A.; Williams, C.; Wilkinson, T.D. Design of hybrid metal-dielectric (Al–TiO2) metasurfaces RGB color filters. *J. Phys. Photonics* **2025**, *7*, 025025. [CrossRef]
18. Kim, D.; Han, J.; Lee, S.; Jang, M.S.; Chung, H. Suppressing Stitching Errors in Full-Sensor-Plane Color Routers via Optical Structural Similarity. *Nanophotonics* **2026**, *15*, e70220. [CrossRef] [PubMed]
19. Shi, Y.; Wan, S.; Wang, Z.; Rao, R.; Li, Z. On-Chip Nonlocal Metasurface for Color Router: Conquering Efficiency-Loss from Spatial-Multiplexing. *Light Sci. Appl.* **2026**, *15*, 66. [CrossRef] [PubMed]
20. Chen, H.; Li, N.; Zhao, Y.; Ou, H.; Wang, Y.; Jing, X.; Zhang, N.; Su, Z.; Huang, L. Maximizing the Chirality of Bound States in the Continuum by Inverse Design. *Photonics Res.* **2025**, *13*, 2054–2064. [CrossRef]
21. Ni, B.; Xu, Z.; Jin, X.; Sheng, T.; Chu, G.; Hou, L.; Yu, Y.; Liu, X.; Xiong, J. Design of Dual Narrow-Band Optical Filter Based on Plasmonic Split-Ring Dimer Metasurface. *IEEE Photonics Technol. Lett.* **2024**, *36*, 969–972. [CrossRef]
22. Wang, B.; Xu, Y.; Wu, Z.; Zhang, Z.; Wang, Q. All-dielectric metasurface-based color filter in CMOS image sensor. *Opt. Commun.* **2023**, *540*, 129485. [CrossRef]

23. Liu, H.-Z.; Wu, J. MWIR narrowband filter based on guided-mode resonance sub-wavelength structure. *J. Electron. Sci. Technol.* **2025**, *23*, 100313. [CrossRef]
24. Maksimov, D.N.; Pankin, P.S.; Kim, D.-W.; Song, M.; Peng, C.; Bogdanov, A.A. Temporal coupled mode theory: From bound states in the continuum to uniguided resonances. *Phys. Rev. B* **2025**, *112*, 235303. [CrossRef]
25. Suh, W.; Wang, Z.; Fan, S. Temporal coupled-mode theory and the presence of non-orthogonal modes in lossless multimode cavities. *IEEE J. Quantum Electron.* **2004**, *40*, 1511–1518. [CrossRef]
26. Chang, C.-C.; Huang, L.; Nogan, J.; Chen, H.-T. Invited Article: Narrowband terahertz bandpass filters employing stacked bilayer metasurface antireflection structures. *APL Photonics* **2018**, *3*, 051602. [CrossRef]
27. Xiang, G.; Zhang, Y.; Lu, X.; Xiong, L.; Zhang, Z.; Yuan, Y. All-dielectric transmissive narrow-band filters adjustable within wide spectral range. *Opt. Commun.* **2025**, *575*, 131280. [CrossRef]
28. Červinka, O.; Ligmajer, F.; Brunn, O.; Horáček, M.; Krátký, S.; Šikola, T. Additive and Subtractive Color Filters Based on Birefringent Dielectric Metasurfaces. *arXiv* **2026**, arXiv:2605.25881.
29. Kim, H.; Kim, M.; Chang, T. Bright and vivid plasmonic color filters having dual resonance modes with proper orthogonality. *Opt. Express* **2018**, *26*, 27403–27417. [CrossRef] [PubMed]
30. Mousavi Khaleghi, S.S. High resolution multicolor holograms encoded into color print images with hybrid dielectric/plasmonic metasurfaces. *Appl. Phys. Lett.* **2025**, *126*, 051102. [CrossRef]

Disclaimer/Publisher's Note: The statements, opinions and data contained in all publications are solely those of the individual author(s) and contributor(s) and not of MDPI and/or the editor(s). MDPI and/or the editor(s) disclaim responsibility for any injury to people or property resulting from any ideas, methods, instructions or products referred to in the content.